Pharmacological inhibition of astrocytic transglutaminase 2 facilitates the expression of a neurosupportive astrocyte reactive phenotype in association with increased histone acetylation

Short Title: Pharmacological inhibition of transglutaminase 2 in astrocytes

Thomas Delgado[1]*, Jacen Emerson[1]*, Matthew Hong[1], Jeffrey W. Keillor[2] and Gail VW Johnson[1#]

[1]601 Elmwood Ave, box 604, Department of Anesthesiology and Perioperative Medicine, University of Rochester, Rochester, NY, 14620, USA

* These authors contributed equally to this work

[2] Department of Chemistry and Biomolecular Sciences, University of Ottawa, Ottawa, ON K1N6N5, Canada

[#]Corresponding author: Gail_Johnsonvoll@urmc.rochester.edu

Key Terms

TG2, Astrocytes, Neurosupportive phenotype, Histone modification

Abstract

Astrocytes play critical roles in supporting structural and metabolic homeostasis in the central nervous system (CNS). CNS injury leads to the development of a range of reactive phenotypes in astrocytes whose molecular determinants are poorly understood. Finding ways to modulate astrocytic injury responses and leverage a pro-recovery phenotype holds promise in treating CNS injury. Recently, it has been demonstrated that ablation of astrocytic transglutaminase 2 (TG2) modulates the phenotype of reactive astrocytes in a way that improves neuronal injury outcomes both *in vitro* and *in vivo*. In an *in vivo* mouse model, pharmacological inhibition of TG2 with the irreversible inhibitor VA4 phenocopies the neurosupportive effects of TG2 deletion in astrocytes. In this study, we provide insights into the mechanisms by which TG2 deletion or inhibition result in a more neurosupportive astrocytic phenotype. Using a neuron-astrocyte co-culture model, we show that VA4 treatment improves the ability of astrocytes to support neurite outgrowth on an injury-relevant matrix. To better understand how pharmacologically altering TG2 affects its ability to regulate reactive astrocyte phenotypes, we assessed how VA4 inhibition impacts TG2's interaction with Zbtb7a, a transcription factor we have previously identified as a functionally relevant TG2 nuclear interactor. The results of these studies demonstrate that VA4 significantly decreases the interaction of TG2 and Zbtb7a. TG2's interactions with Zbtb7a, as well as a wide range of other transcription factors and chromatin regulatory proteins, suggest that TG2 may act as an epigenetic regulator to modulate gene expression. To begin to understand if TG2-mediated epigenetic modification may impact astrocytic phenotypes in our models, we interrogated the effect of TG2 deletion and VA4 treatment on histone acetylation and found significantly greater acetylation in both experimental groups. Consistent with these findings, previous RNA-sequencing and our present proteomic analysis also supported a predominant transcriptionally suppressive role of TG2 in astrocytes. Our proteomic data additionally unveiled pronounced changes in lipid and antioxidant metabolism in astrocytes with TG2 deletion or inhibition, which likely contribute to the enhanced neurosupportive function of these astrocytes.

Introduction

Astrocytes are unique and versatile cells of the central nervous system (CNS). In homeostatic conditions, astrocytes maintain the blood-brain barrier, regulate the extracellular matrix (ECM), and provide crucial metabolic support for neurons, among other functions [1-3]. Inflammatory and stress signals, whether from injury, infection, or other sources, cause astrocytes to take on a range of phenotypes from neuroprotective to neurotoxic, although the exact molecular determinants of these phenotypes are poorly understood [4-12]. Our lab has previously identified the protein transglutaminase 2 (TG2) as a key factor in modulating the phenotype of reactive astrocytes [13-17].

TG2 is a widely expressed, multi-functional protein in the transglutaminase family and is the most highly expressed transglutaminase in the brain. TG2 has been studied mostly as a transamidating enzyme, which catalyzes the incorporation of an amine into a glutamine of the acceptor protein [18-22]. This reaction requires calcium which stabilizes TG2 in a catalytically active, open conformation [23,24]. Conversely, GTP/GDP stabilizes TG2 in a closed, catalytically inactive conformation which, due to the relatively high intracellular concentrations of GTP/GDP compared to calcium, is the predominant intracellular conformation of TG2 [25,26]. In the closed conformation, TG2 can function as a scaffold for protein-protein interactions at the cell surface and in the nucleus, with well-described roles in cell-ECM interactions and chromatin regulation [18,20,21,25,27-30]. Additionally, the TG2 promoter contains transcription factor binding sites associated with inflammation and hypoxia; therefore, TG2 expression is often greatly increased in injury conditions, allowing TG2 to have significant influence on cellular injury responses through its transamidating or scaffolding roles [31-33].

We have previously shown that astrocytic TG2 greatly influences neuronal survival and recovery in multiple injury models. TG2 deletion makes astrocytes more resilient to oxygen-glucose deprivation and improves their ability to protect neurons in these conditions [13,17,34]. *In vivo*, mice with TG2 selectively knocked out of astrocytes show significantly faster motor function recovery after spinal cord injury (SCI) compared to wild type (WT) mice [14]. To isolate potential mechanisms underlying this intriguing finding, we modeled axonal regeneration *in vitro* using a neurite outgrowth assay in which we grew neurons on an injury-

relevant, growth-inhibitory matrix comprised of chondroitin sulfate proteoglycans (CSPGs) and paired them with TG2 knockout (TG2-/-) or WT astrocytes. CSPGs are an important component of the post-SCI environment as they are densely deposited in and around the lesion core and inhibit axonal regeneration across the lesion [11,35,36]. We found that TG2-/- astrocytes facilitated neurite outgrowth across the simulated lesion matrix to a greater extent than WT astrocytes [15]. Given these findings, we hypothesize that the mechanisms through which TG2-/- astrocytes can better promote neurite outgrowth on a growth-inhibitory matrix are also contributing to the enhanced functional recovery of astrocytic TG2-/- mice after SCI; however, the exact molecular and functional aspects of these astrocytic changes have yet to be identified.

To further study the role of TG2 on astrocytic stress responses, we have inhibited TG2 using our small molecule inhibitor VA4 [37]. VA4 irreversibly modifies TG2 function by binding and blocking active site residues necessary for its catalytic activity and "locking" TG2 in its open conformation, thereby also potentially altering protein scaffolding function associated with its closed conformation [23,26,38-40]. Previously, we demonstrated that VA4 treatment of WT astrocytes phenocopied functional effects of astrocytic TG2 deletion. *In vitro*, both TG2 deletion and VA4 treatment significantly improved astrocyte survival after an ischemic insult [16], while *in vivo*, VA4 treatment of WT mice significantly improved motor function recovery after SCI, compared to vehicle treatment, to an extent similar to that observed in mice with astrocyte-specific TG2 deletion [14]. These data indicate that VA4 treatment, like TG2 deletion, improves the resilience of astrocytes in stress conditions and promotes a neurosupportive phenotype in reactive astrocytes after CNS injury. Our present study extends our mechanistic understanding of the neurosupportive changes that occur in astrocytes with TG2 deletion and inhibition.

Methods and Materials

Animals

All mice and rats were maintained on a 12-hour light/dark cycle with food and water available ad libitum. The procedures with animals were in accordance with guidelines established by the University of Rochester Committee on Animal Resources and were carried out with approval from the Institutional Animal Care and Use

Committee (protocol # 2007-23ER). WT C57BL/6 mice were originally purchased from Charles River Laboratories. Our TG2-/- mice on a C57Bl/6 background were described previously and have been continuously bred in house [13]. Timed-pregnant Sprague Dawley rats were obtained from Charles River Laboratories.

Cell Culture

Primary astrocytes were cultured between post-natal days 0 to 1 (P0-P1) from either WT C57BL/6 or TG2-/- mouse pups as previously described [13]. In brief, P0-P1 mouse pups were rapidly decapitated, the brains were collected and dissected, meninges removed, and cortical hemispheres were collected. Following trituration, cells were plated onto culture dishes in MEM supplemented with 10% FBS (Atlas Biologicals, F-0500-DR), 33 mM glucose, 1 mM sodium pyruvate (Gibco, 11360-070), and 0.2% Primocin (Invivogen ant-pm-05) (glial MEM). Cortical tissues were pooled from all pups in a litter during plating, so our astrocyte cultures were mixed sex. Twenty-four hours after plating, the dishes were shaken vigorously and rinsed to remove debris and other cell types. Astrocytes were maintained at 37°C/5% CO_2 for 7-8 days, frozen in glial MEM containing 10% DMSO, and stored in liquid nitrogen. For experiments, astrocytes were thawed, grown, and passaged in glial MEM, and only cultures on 2nd or 3rd passages at no greater than 90% confluency were used for final data acquisition.

Primary cortical neurons were prepared from Sprague Dawley rat embryos at embryonic day 18 (E18) and cultured as previously described with some modifications [41]. To prepare the coverslips/wells, poly-D-lysine (Sigma P6407) was diluted in PBS to a concentration of 20 µg/mL and added to the wells for 4 hours. The wells were either rinsed and stored with PBS, or after rinsing, CSPGs (Millipore, CC117) in PBS (2.5 µg/mL) were added and incubated overnight to coat the coverslips. All wells and coverslips were rinsed with PBS prior to plating the neurons. To prepare the neurons, pregnant rats were euthanized using CO_2, followed by rapid decapitation in accordance with NIH Animal Research Advisory Committee guidelines. Embryos were removed, rapidly decapitated, brains were extracted, cerebral cortices dissected, and meninges were removed. Cerebral cortices were then digested in trypsin-EDTA (0.05%) (Corning, 25-053-Cl) for 15-20 min in a 37°C water bath. Following gentle trituration, neurons were plated in neuron plating medium consisting of MEM (Gibco, 42360032) supplemented with 5% FBS, 20 mM glucose, and 0.2% Primocin at a density of 12,000 cells/cm^2 on the coated coverslips. Cortical tissues were pooled from all pups in a litter during plating, so our neuron cultures

were mixed sex. Four to five hours after plating, the medium was replaced with Neurobasal medium (Gibco, 21103-049) containing 2% B27 (Gibco, 17504-044), 0.5 mM Glutamax (Gibco, 35050-061) and 0.2% Primocin (neuron growth medium). Neurons were incubated at 37°C/5% CO_2 and experiments begun at days *in vitro* (DIV) 1.

HEK 293TN cells were thawed and grown at 37°C/5% CO_2 in DMEM (Gibco 11995-065) supplemented with 10% FBS, 1x GlutaMAX (Gibco 35050-061), and 4.5 µg/mL gentamicin (Gibco 15710-064). Cells were grown to confluency and passaged using trypsin-EDTA (0.05%) (Corning, 25-053-Cl) at least once before use in immunoprecipitation (IP) experiments.

VA4 treatment

Cultured cells were treated with 10 µM VA4 or 0.04% DMSO for vehicle control. For IP experiments, HEK 293TN cells were treated with VA4 12 hours after transfection (48 hours before protein collection). For immunoblot experiments, astrocytes were treated with VA4 for 48 hours before protein collection. For neurite outgrowth studies, astrocytes were pre-treated with VA4 for 4 days before being paired with neurons. The astrocyte cultures received a complete medium change and replacement of VA4 after 2 days of incubation. After pairing with DIV 1 neurons, astrocytes were treated with VA4 throughout the experiment, from DIV 1 to DIV 5 of neuron culture, receiving a complete medium change and VA4 replacement at DIV 3.

Neurite Outgrowth Analyses

WT and TG2-/- astrocytes, treated with VA4 or DMSO vehicle, were seeded onto transwell inserts (6.5 mm) with a membrane pore size of 1.0 µm (Grenier Bio-One 665610) in glial MEM 48 hours prior to pairing with the neurons. The astrocyte transwell cultures were switched into supplemented neurobasal medium 24 hours before pairing. On neuron DIV 1, the inserts were placed over the neuron coverslips of a 12-well plate and the neurons received a half medium change with astrocyte-conditioned neurobasal medium. The cell pairs were incubated for 96 hours, and neuron coverslips were collected for analysis of neurite outgrowth.

Neuron coverslips from the transwell co-cultures were washed three times with PBS, followed by fixation with 2% paraformaldehyde and 4% sucrose in PBS for 5 min. After three washes with PBS, the cells were permeabilized with 0.25% Triton X-100 in PBS and blocked with PBS containing 5% BSA and 0.3 M glycine.

Rabbit anti-MAP2 (Cell Signaling #8707S) was diluted in blocking buffer (1:200) and incubated overnight on the coverslips. The next day, the coverslips were washed three times and incubated in Alexa Fluor 594 donkey anti-rabbit (Invitrogen A21207) for 1 hour. Coverslips were then counterstained with Hoechst 33342 (1:10,000) and mounted using Fluoro-gel in TES Buffer (Electron Microscopy Sciences, 17985-30). The slides were imaged using a Zeiss Observer D1 microscope with a 40x objective.

Ten to fifteen neurons per coverslip were imaged for each experimental group. Images were processed by Image J Fiji using the Simple Neurite Tracer (SNT) plugin. Neurites were traced using a scale of 6.7 pixel/µm. For the max neurite length studies, the longest neurite of each neuron was recorded.

Constructs

The use of V5-tagged human TG2 in pcDNA and in the lentiviral vector FigB has been described previously [41,42]. The FLAG-tagged Zbtb7a construct was purchased from Origene (RC222759).

Immunoblotting

For protein collection, cells were lysed and collected in IP lysis buffer (150mM NaCl, 50 mM Tris-HCl, 1 mM EDTA, 1 mM EGTA, 0.5% NP-40 in PBS). Protein concentrations were measured using a BCA assay. Samples were prepared at 1 µg/ 1µL in 1x SDS containing IP lysis buffer and boiled at 100°C for 10 min. Protein samples were resolved on 12% SDS-PAGE gels and proteins transferred to a nitrocellulose or PVDF membrane. Membranes were blocked in blocking buffer, 5% milk in Tris-Buffered Saline with Tween 20 (TBS-T) (20 mM Tris base, 137 mM NaCl, 0.05% Tween 20), for 1 hour at room temperature. After blocking, primary antibodies against FLAG tag (CST 8146S), V5 tag (CST 13202S), GAPDH (Proteintech 60004-1-Ig), acetylated histone H3 K9 (CST 9649S), or beta tubulin (rabbit polyclonal antibody, Proteintech 10094-1-AP) were added to the blots in fresh blocking buffer and incubated at 4°C overnight. The next day blots were washed with TBS-T and incubated for 1 hour at room temperature with HRP-conjugated secondary antibody in blocking buffer. The blots were washed with TBS-T before being visualized with an enhanced chemiluminescence reaction. ImageJ was used to quantify the intensity of each band, and all values were normalized to GAPDH or beta tubulin levels.

Co-immunoprecipitation

For immunoprecipitation (IP), HEK 293TN were transfected with V5-TG2 and FLAG-Zbtb7a constructs using PolyJet transfection reagent (Signagen SL100688) following the manufacturer's protocol. The cells were treated with VA4 12 hours after transfection and collected 48 hours after VA4 treatment. The cells were lysed and collected in IP lysis buffer (150mM NaCl, 50 mM Tris-HCl, 1 mM EDTA, 1 mM EGTA, 0.5% NP-40 in PBS). Protein concentrations were measured using a BCA assay. A 300 µg aliquot of lysate was immunoprecipitated with 4 µL of rabbit anti-V5 tag antibody (CST 13202S). After addition of primary antibody, the samples were incubated on a rotator at 4 °C overnight. IgG control samples were incubated with an equivalent amount of normal rabbit (Millipore 12-370) IgG antibody. After 18 hours, 30 µL of Pierce protein A/G magnetic agarose beads, (Thermo Scientific 78609) washed in IP wash buffer (2mM EDTA, 0.1% NP-40 in PBS) and blocked in 1% BSA in PBS, were added. After a 4-hour incubation, rotating at 4 °C, the samples were thoroughly washed in IP wash buffer and then in IP lysis buffer. After washing, beads were incubated in 30 µL of 2.5x SDS in IP lysis buffer for 10 min at 100 °C. Samples were then immunoblotted as described above. For quantification, ImageJ was used to measure the intensity of FLAG and V5 bands in each lane and the FLAG signal was normalized to that of V5.

Sample Preparation for Liquid Chromatography with tandem mass spectrometry (LC-MS/MS)

Cell Culture

Astrocytes were cultured in 60 mm dishes for 7 days in their second passage, with a half-media change every 3 days. They were then washed with PBS, trypsinized, washed again, and frozen as cell pellets prior to further analysis. For VA4 experiment, WT astrocytes were cultured in 60 mm dishes for 7 days in their second passage, with a half-media change on DIV 3. On DIV 5, they received a full media change with 10 µM VA4 or 0.04% DMSO. On DIV 7, they were then processed as above and frozen as cell pellets. Cell pellets were submitted to the URMC Mass Spectrometry Core.

Sample Preparation

Cell lysis was performed by adding 300 µL of 5% SDS, 100 mM triethylammonium bicarbonate (TEAB) per 6 x 10^6 cells. Samples were vortexed and then sonicated (QSonica) for 5 cycles, with a 1 min resting period on ice after each cycle. Lysates were then centrifuged at 15,000 x g for 5 min to collect cellular debris, and the

supernatant was collected. Protein concentration was determined by BCA (Thermo Scientific), after which samples were diluted to 1 mg/mL in 5% SDS, 50 mM TEAB.

Twenty-five micrograms of protein from each sample was reduced with dithiothreitol to 2 mM, followed by incubation at 55°C for 60 min. Iodoacetamide was added to 10 mM and incubated in the dark at room temperature for 30 min to alkylate the proteins. Phosphoric acid was added to 1.2%, followed by six volumes of 90% methanol, 100 mM TEAB. The resulting solution was added to S-Trap micros (Protifi) and centrifuged at 4,000 x g for 1 min. The S-Traps containing trapped protein were washed twice by centrifuging through 90% methanol, 100 mM TEAB. 1 µg of trypsin was brought up in 20 µL of 100 mM TEAB and added to the S-Trap, followed by an additional 20 µL of TEAB to ensure the sample did not dry out. The cap to the S-Trap was loosely screwed on but not tightened to ensure the solution was not pushed out of the S-Trap during digestion. Samples were placed in a humidity chamber at 37°C overnight. The next morning, the S-Trap was centrifuged at 4,000 x g for 1 min to collect the digested peptides. Sequential additions of 0.1% trifluoroacetic acid (TFA) in acetonitrile (ACN) and 0.1% TFA in 50% ACN were added to the S-trap, centrifuged, and pooled. Samples were frozen and dried down in a Speed Vac (Labconco), then re-suspended in 0.1% trifluoroacetic acid prior to analysis.

Samples related to Fig. 5 a,b,e were reconstituted in TEAB to 4 mg/mL in 100mM TEAB, then labeled with tandem mass tag (TMT) 10plex reagents (Thermo Scientific) following the manufacturer's protocol. Briefly, TMT tags were removed from the -20C freezer and allowed to equilibrate to RT for 5 min, after which, 22 µL of ACN was added to each tag. 20 µL of individual TMT tags were added to respective samples and the reactions were carried out at RT for 1 hour, after which, the reaction was quenched by adding 5% hydroxylamine. All 10 samples were combined and dried down in a speed vac prior to high-pH fractionation.

Labeled peptides were fractionated using homemade C18 spin columns. The C18 was activated by two 50 µL washes of ACN via centrifugation followed by equilibration by two 50 µL washes of 10mM ammonium hydroxide (NH_4OH). Peptides were resuspended in 50 µL of 10mM NH_4OH and added to the spin column. After centrifugation, the column was washed twice with 10mM NH_4OH. Fractions were eluted off the column with centrifugation by stepwise addition of 10mM NH_4OH with increasing percentage of ACN as follows: 2, 3.5, 5, 6.5, 8, 9.5, 11, 12.5, 14, 15.5, 17, 18.5, 20, 21.5, 27, 50%. The 16 fractions were concatenated down to 8 by

combining fractions 1 and 9, 2 and 10, 3 and 11, etc. Fractionated samples were frozen, dried down in the speed vac, and brought up in 0.1% TFA prior to mass spectrometry analysis.

LC-MS/MS

Data Collection

Peptides were injected onto a homemade 30 cm C18 column with 1.8 um beads (Sepax), with an Easy nLC-1200 HPLC (Thermo Fisher), connected to a Fusion Lumos Tribrid mass spectrometer (Thermo Fisher). Solvent A was 0.1% formic acid (FA) in water, while solvent B was 0.1% FA in 80% ACN. Ions were introduced to the mass spectrometer using a Nanospray Flex source operating at 2 kV. Data were collected by two different methods: data-dependent acquisition (DDA) with TMT-MS3 and data-independent acquisition (DIA).

For the data collected with DDA TMT-MS3 (see Supplementary Table S1), the gradient began at 3% B for 2 min, increased to 10% B over 7 min, increased to 38% B over 94 min, then ramped up to 90% B over 5 min where it was held at 90% B for 3 min before returning to 0% B for 2 min and re-equilibrating for 7 min, for a total runtime for 120 min. The Fusion Lumos was operated in data-dependent mode, with MultiNotch Synchronized Precursor Selection MS3 (SPS-MS3) enabled to increase quantitative accuracy [43]. The cycle time was set to 3 seconds with monoisotopic precursor selection set to 'Peptide'. MS1 scans were acquired in the Orbitrap at a resolution of 120,000 at *m/z* of 200 over a range of 400-1500 *m/z*, with an AGC target of 4e5, and a maximum ion injection time of 50 ms. Precursor ions with a charge state of 2-5 were selected for fragmentation by collision-induced dissociation (CID) using a collision energy of 35% and an isolation width of 1.0 *m/z*. MS2 scans were acquired in the ion trap with an AGC target of 1e4 and a maximum ion injection time of 35 ms. Dynamic exclusion was set to filter precursor ions after 1 time with a duration of 45 seconds and high and low mass tolerances of 10 ppm using a maximum intensity threshold of 1e20 and minimum intensity threshold of 1e4. MS3 scans were performed by selecting the 10 most intense fragment ions between 400-200 *m/z* with an isolation width of 2 Da, excluding any ions that were 40 *m/z* less or 10 *m/z* greater than the precursor ions, which were then fragmented using higher energy collisional dissociation (HCD) using a collision energy of 60%. MS3 ions were detected in the Orbitrap with a resolution of 50,000 at *m/z* 200 over a range of 100-300 *m/z* with an AGC target of 1e5, a normalized AGC target of 200%, and a maximum ion injection time of 100 ms.

For the data collected with data-independent acquisition (DIA) (Fig. 5c,d,f) (see Supplementary Tables S2,S3), the gradient began at 4% B for 2 min, increased to 28% B over 66 min, increased to 38% over 7 min, increased to 90% B over 5 min and was held at 90% B for 3 min to wash the column, before returning to 0% B over 2 min and re-equilibrating for 5 min, for a total runtime of 90 min. The Fusion Lumos was operated in data-independent acquisition (DIA) mode, with MS1 scans acquired in the Orbitrap at a resolution of 60,000 over a range of 395-1005 *m/z*, with an AGC target of 4e5, and a maximum injection time of 50 ms. MS2 scans were acquired in Orbitrap with a resolution of 15,000 over a range of 200-2000 *m/z*, with a maximum ion injection time of 23 ms, HCD collision energy set to 33%, an AGC target of 4e5, and normalized AGC of 800%. Precursor ions were sampled using a staggered windowing scheme of 8 *m/z* with 4 *m/z* overlaps for a total of 75 windows between MS1 scans.

Data Analysis

For the data collected with DDA TMT-MS3, raw data were searched using the SEQUST search engine within the Proteome Discoverer platform, version 2.4 (Thermo Scientific), using the UniProt Mouse database (downloaded 4/27/2021). Trypsin was selected as the enzyme allowing up to 2 missed cleavages, with an MS1 mass tolerance of 10ppm, and an MS2 mass tolerance of 0.6 Da. Carbamidomethylation of cysteine and TMT on lysine and peptide N-terminus were set as fixed modifications. Oxidation of methionine was set as a variable modification. Percolator was used as the FDR calculator, filtering out peptides with a q-value of greater than 0.01. Reporter ions were quantified using the 'Report Ions Quantifier' node with an integration tolerance of 20 ppm and integration method set to 'most confident centroid'. Protein abundances were calculated by summing the signal to noise of the report ions from each identified peptide. P-values were measures using a student's t-test within Proteome Discoverer.

For the data collected with DIA, raw data were searched with DIA-NN version 1.8.1 (https://github.com/vdemichev/DiaNN) [44]. For all experiments, data analysis was carried out using library-free analysis mode in DIA-NN. To annotate the library, the mouse UniProt 'one protein sequence per gene' database (UP000000589_10090, downloaded 9/12/2021) was used with 'deep learning-based spectra and RT prediction' enabled. For precursor ion generation, the maximum number of missed cleavages was set to 1, cysteine

carbamidomethylation set as a fixed modification, maximum number of variable modifications to 1 for Ox(M), peptide length range to 7-30, precursor charge range to 2-3, precursor *m/z* range to 400-1000, and fragment *m/z* range to 200-2000. The quantification was set to 'Robust LC (high precision)' mode with normalization set to RT-dependent, MBR enabled, protein inferences set to 'Genes', and 'Heuristic protein inference' turned off. MS1 and MS2 mass tolerances, along with the scan window size were automatically set by the software. Precursors were subsequently filtered at library precursor q-value (1%), library protein group q-value (1%), and posterior error probability (20%). Protein quantification was carried out using the MaxLFQ algorithm as implemented in the DIA-NN R package (https://github.com/vdemichev/diann-rpackage) and the number of peptides quantified in each protein group was counted as implemented in the DiannReportGenerator R Package (https://github.com/URMC-MSRL/DiannReportGenerator)[45]. Downstream processing and statistical analyses were performed using the Perseus software [46]. Specifically, proteins IDs were filtered to only allow proteins identified with 2 or more peptides in at least two samples in one biological group. Missing values were then imputed from a normal distribution with a standard deviation of 0.3 and a downshift of 1.8 and a two-sample student's t-test was performed on the imputed data. Perseus output was converted to excel format using the ProteinReportr R package (https://github.com/URMC-MSRL/ProteinReportr).

Protein Differential Expression Analysis

Differentially expressed proteins were identified using pairwise t-tests followed by Benjamini-Hochberg (BH) FDR correction. Data was sorted by log2 fold change and adjusted p value. Log2 fold change values between 0.5 and -0.5 and adjusted p values > 0.05 were excluded from further analysis. Differential expression was presented in volcano plots, which were generated using GraphPad Prism 10. A Venn diagram was generated using BioVenn (https://doi.org/10.1186/1471-2164-9-488).

Gene Ontology Analyses

Sorted differentially expressed gene symbol lists were analyzed using DAVID GO Biological Process (https://doi.org/10.1038/nprot.2008.211). The enrichment data was extracted for generating dot plots using ggplot2 package in R 4.3.2. Gene lists were also analyzed by Enrichr to yield consensus transcription factor

enrichments based on ENCODE and ChEA databases of multi-omic, chromatin immunoprecipitation data (doi: 10.1186/1471-2105-14-128, doi: 10.1093/nar/gkw377, https://doi.org/10.1002/cpz1.90).

Statistical Analysis

GraphPad Prism 10 was used to report the raw data and perform statistical analysis. Outliers were evaluated using ROUT with Q=1% for all figures. Normality was tested using a Shapiro-Wilk test. The mean values and standard error of the mean were calculated for each group. For significance testing, an unpaired *t*-test was used in Figures 2-4 and a Kruskal Wallis Test in Figure 1, and levels of significance were set at *$p < 0.05$, **$p < 0.01$, ***$p < 0.001$, ****$p < 0.0001$. Details of statistical analyses are given in Supplemental Table S5.

Results

VA4 Neurite Outgrowth

Recently, we demonstrated that TG2 deletion in astrocytes enhances their ability to support neurite outgrowth on a growth-inhibitory matrix, which simulates the extracellular matrix of a SCI lesion core [15]. This finding provides potentially important insight into the mechanisms underlying the enhanced functional recovery of astrocytic TG2 deleted mice after SCI [14]. Notably, we could phenocopy this effect by treating mice with VA4 after SCI (14). Therefore, we asked whether TG2 inhibition by VA4 treatment of astrocyte cultures could replicate our previous neurite outgrowth data with TG2-/- astrocytes. For these experiments, WT astrocytes were grown on transwells and treated with VA4 or DMSO vehicle. They were then paired with neurons seeded on a growth-inhibitory matrix comprised of CSPGs on DIV 1 of neuron culture (Fig. 1a). As expected, the presence of WT astrocytes (either VA4-treated or vehicle-treated) resulted in significantly greater neurite outgrowth on CSPGs compared to unpaired neurons. Similar to the enhanced neurite outgrowth observed in the presence of TG2-/- astrocytes [15], neurons paired with VA4-treated astrocytes promoted significantly greater neurite outgrowth compared to vehicle-treated astrocytes (Fig. 1b,c). Importantly, VA4 treatment of neurons alone did not affect their neurite outgrowth on a growth-supportive poly D Lysine (PDL) or CSPG matrix (Fig. S1), and VA4 treatment of TG2-/- astrocytes showed no added effect on their ability to support neurite outgrowth on a CSPG matrix (Fig. S2).

Immunoprecipitation of TG2 and Zbtb7a after VA4 Treatment

The ability of TG2 to regulate gene expression has been well-described in the literature and our previous data suggest that this role of TG2 is integral to its ability to influence injury response across cell types [14,17,18,28,42,47-55]. We hypothesize that TG2 is an important regulator of neurosupportive gene expression in reactive astrocytes; however, the mechanisms by which it regulates gene expression and the functionally significant genes impacted in astrocytes have not been fully delineated. We previously posited that the interaction between TG2 and Zbtb7a, a transcription factor that is ubiquitous throughout the nucleus, is an important contributor to the ability of TG2 to regulate gene expression in reactive astrocytes [15]. Having established the ability of VA4 treatment to phenocopy the effects of TG2 deletion in our neurite outgrowth model, we asked whether VA4 could alter the interaction between TG2 and Zbtb7a. To address this question, HEK cells were transfected with V5-tagged TG2 and FLAG-tagged Zbtb7a, followed by VA4 or vehicle-only treatment [15]. Immunoprecipitation (IP) of TG2 from the VA4-treated cell lysates resulted in significantly less pull down of Zbtb7a compared to vehicle-only treated cells (Fig. 2), demonstrating reduced interaction between these proteins.

Histone Acetylation in WT and TG2-/- Astrocytes

Previous data from our lab suggest that TG2 has both a minor activating effect and a predominant repressive effect on gene expression in astrocytes [14,17], and we hypothesize that interactions with Zbtb7a and other epigenetic regulators facilitates TG2's transcriptional effects. Concordantly, Zbtb7a has been independently shown to facilitate both transcriptional activation and repression in association with its ability to promote accessibility of transcription factors to gene promoters and its ability to bind to repressive chromatin regulatory complexes [56]. Previous yeast-two hybrid and interactome analyses revealed that TG2 and Zbtb7a both interact with components of Sin3a, a transcriptional repressor complex that facilitates chromatin modifications by HDAC1 and HDAC2 [15,57-59]. Notably, the Sin3a complex is an important regulator of injury responses across cell types [60-62]. With these data in mind, we hypothesized that TG2 limits the chromatin accessibility of neurosupportive genes in reactive astrocytes in part through regulating histone acetylation. Acetylated H3K9 (H3K9ac) localizes to active gene promoters and is associated with enhanced transcriptional activity [63]. Therefore, we measured global H3K9ac levels in WT and TG2-/- astrocytes and found that TG2-/- astrocytes had significantly higher acetylation levels than WT astrocytes at steady state in glial media (Fig. 3).

Histone Acetylation after VA4 Treatment in WT Astrocytes

Given the significantly higher levels of H3K9ac in TG2-/- astrocytes, we asked whether VA4 treatment of WT astrocytes could replicate this epigenetic effect. VA4-treated astrocytes exhibited a significant increase in H3K9ac levels compared to vehicle-treated astrocytes (Fig. 4), comparable to the levels observed in TG2-/- astrocytes (Fig. 3).

Differential Proteomic Analysis in TG2-/- and VA4-treated Astrocytes

Our lab has previously analyzed transcriptional differences between TG2/- and WT astrocyte cultures using RNA-sequencing [17]. To extend these findings and provide more insight into the functional differences observed in astrocytes with TG2-/- deletion or inhibition that may explain their neurosupportive phenotype, we analyzed the proteome of TG2-/- astrocytes and VA4-treated astrocytes in steady-state conditions (Fig. 5). Differential analyses comparing TG2-/- and VA4-treated astrocytes to WT and vehicle-treated astrocytes, respectively, show strong enrichments in lipid metabolic pathways through GO Biological Process (Fig. 5b,d). Additionally, both analyses show top enrichments of genes associated with NFE2L2, or NRF2, as well as Zbtb7a, through transcription factor gene ontology categories (Fig. 5e,f). While VA4 astrocytes show a wider range of differentially regulated proteins compared to the TG2-/- astrocytes, TG2-/- astrocytes share the majority, about 70%, of their differentially regulated proteins with VA4-treated astrocytes (Fig. 5g). Replicate proteomic analysis of TG2-/- and WT astrocytes using data independent acquisition (DIA) is shown in Fig. S4. All data from proteomic analyses are included as supplemental tables (Table S1-S4; excel files).

Discussion

Herein, we show that VA4 treatment of WT astrocytes phenocopies the ability of TG2-/- astrocytes to promote greater neurite outgrowth on a growth-inhibitory CSPG matrix compared to untreated WT astrocytes. The implications and limitations of our neurite outgrowth findings were discussed in depth in our previous paper [15]. Chiefly, our neurite outgrowth data suggest that TG2 deletion or inhibition in astrocytes improves their ability to support highly energy-dependent processes in neurons in a stress context. CSPGs have been extensively studied in the context of SCI; and intriguing data suggest that their growth-inhibitory effect on neurons may in part be due to inhibition of autophagic processes, which may induce energetic and proteostatic stress [64]. Astrocytes can

respond to neuronal stress cues by upregulating neurosupportive functions, and this response is likely altered in astrocytes in which TG2 is deleted or inhibited. The underlying astrocytic functional differences that contribute to our neurite outgrowth findings may also contribute to the improved motor function recovery after SCI observed in VA4-treated and astrocytic TG2-/- mice by enhancing axonal regeneration [15]. This study provides insight into the mechanisms through which TG2 acts to influence astrocytic response to stress and which astrocytic functions are predominantly affected by TG2 deletion or inhibition.

TG2 is an injury-responsive protein whose function depends on many factors, including intracellular localization. While TG2 is predominantly cytosolic, it migrates in and out of the nucleus (depending on cell type) in response to injury to influence gene expression [34,41,42,50,60]. Our lab and others have shown that TG2's regulation of gene expression can be mediated through its nuclear interactions, where it may act as a protein scaffold to bring together transcription factors and chromatin regulatory complexes or as an enzyme to catalyze post-translational modifications of epigenetic proteins such as histones [21,22,29,42,47-53]. In astrocytes, TG2 is primarily associated with transcriptional repression, and given the aforementioned functional effects of astrocytic TG2 deletion, we hypothesize that nuclear interactions by TG2 attenuates the upregulation of neurosupportive signaling pathways in astrocytes during stress.

In line with our hypothesis, inhibition of astrocytic TG2 function by VA4 replicates the neurosupportive effects of TG2-/- astrocytes. VA4 binds to TG2's catalytic domain, blocks TG2's catalytic activity, and locks TG2 in the open conformation, which may prevent scaffolding interactions that are dependent on its closed conformation [23]. VA4 therefore putatively limits TG2's ability to interact with a range of nuclear proteins, so we tested whether VA4 alters the interaction of TG2 and Zbtb7a, a transcription factor that regulates chromatin accessibility and that we previously identified as a TG2 nuclear interactor [15,17,54]. We confirmed that VA4 treatment of astrocytes significantly decreased TG2 binding to Zbtbt7a, suggesting that TG2 requires at least its catalytic domain and/or its closed conformation to bind Zbtb7a. Notably, previous data from our lab using overexpression constructs of mutant TG2 with deficient catalytic and GTP-binding ability suggest that TG2 can still regulate gene expression, independent of its catalytic activity [50]. To what degree TG2's open and closed

conformations contribute to its ability to bind to and scaffold between nuclear proteins, and more specifically, which protein domains are important for these interactions, remain open questions.

Interestingly, both TG2 and Zbtb7a can bind to proteins within the Sin3a complex, a transcriptional repressor complex important for gene regulation in response to environmental stress [15,57,59,61]. Sin3a complex proteins associate with the histone deacetylases HDAC1 and HDAC2 to decrease chromatin accessibility [58]. Therefore, we measured acetylated histone levels, markers of chromatin accessibility and gene transcription, in WT and TG2-/- astrocytes. For these studies, we specifically measured the levels of H3K9ac, as this histone modification is well-established as a mediator of increased chromatin accessibility and transcriptional activity [63]. Both TG2 deletion and VA4 treatment significantly increased the level of H3K9ac in astrocytes. These findings agree with previous RNA sequencing results showing gene upregulations in injured spinal cord tissue from mice with astrocytic TG2 deletion and a predominant upregulation of genes in cultured TG2-/- astrocytes compared to wild type controls [14,17].

Similar to our previous RNA sequencing data, our present proteomic analysis of astrocyte cultures shows that TG2 deletion leads to a predominant protein upregulation. Interestingly, however, this trend was not observed in the VA4-treated vs vehicle-treated WT astrocyte culture comparison, which shows a much wider range of differentially regulated proteins with no clear preference for up- or down-regulation. This difference may be partly explained by the acute nature of inhibiting TG2 function relative to TG2-/- astrocytes, but this also likely suggests that VA4 has off-target binding effects that need to be further investigated. Strikingly, however, both the TG2-/- and VA4 proteomic comparisons showed strong enrichments in lipid metabolic pathways, consistent with our RNA-seq data of injured spinal cord tissue from astrocytic TG2-/- mice [14]. Following our hypothesis that TG2 acts primarily in an epigenetic role to control astrocytic injury responses, we also analyzed transcription factor pathway enrichments in our proteomic data, which surprisingly showed top enrichments in NFE2L2, or NRF2, pathways. NRF2 is a stress-responsive transcription factor and has a master regulatory role in antioxidant production, among other cell-protective roles relevant to CNS injury [65], and NRF2 serves as an important mediator for astrocytic response to neuronal stress [66-68]. Additionally, proteins associated with Zbtb7a were among the top significantly enriched transcription factor categories in both TG2-/- and VA4 datasets (Fig. 5e,f).

The transcriptional and proteomic changes from deletion or inhibition of TG2 appear to be dynamic and perhaps very context-dependent so that, across different replicates and analyses, the same genes or proteins are not always differentially expressed, but our data show that the enriched pathways across datasets are remarkably consistent. However, it is worth mentioning that in a re-analysis of our previous *in vitro* RNA-seq data from TG2-/- astrocytes we found a uniquely top enrichment in genes associated with polycomb repressor complex 2 (PRC2) (Fig. S3), which is a transcriptionally repressive chromatin modifying complex that may play a role in TG2-mediated transcriptional repression [69]. A more recent run of RNA-sequencing also replicated this enrichment (see Supplemental Table S4). Although this same enrichment category was not found in our proteomic data, it is interesting to note there were consistently significant protein enrichments in H3K27me3 categories, which are histone marks only known to be catalyzed by PRC2 [69]. Across our RNA-sequencing and proteomic data, including the VA4 dataset, PRC2 and/or H3K27me3 categories were enriched primarily in downregulated targets. Conversely, in proteomic data of TG2-/- and VA4-treated astrocytes, pathways associated with Zbtb7a were consistently enriched in upregulated proteins.

The TG2-Zbtb7a-Sin3a interaction represents a novel and potentially important mechanism that contributes to stress-induced gene regulation by TG2, likely among other contributing players (e.g. PRC2) [15,59]. The Sin3a complex is an important regulator of gene expression during stress, particularly in hypoxic stress [60-62]. Indeed, it regulates the vast majority of the transcriptional response to hypoxia and is necessary for a complete response [61]. Our data suggest that TG2 facilitates histone deacetylation, but as TG2 lacks a canonical DNA binding motif, this effect is likely mediated through TG2 partnering with DNA-binding transcription factors, like Zbtb7a, and with proteins capable of recruiting a histone de-acetylase, like members of the Sin3a complex. With TG2 deletion or inhibition in astrocytes, repressive epigenetic complexes like Sin3a may have reduced occupancy and activity near stress-induced neurosupportive genes. Figure 6 summarizes this proposed mechanism by which TG2 may mediate the neurosupportive status of reactive astrocytes.

Data Availability Statement: All raw data are in Supplementary Tables S1-S4.

Acknowledgments: The authors would like to thank Joel Rodwell-Bullock for his assistance. This work was supported by NIH grant R21NS119673. This research has been facilitated by the University of Rochester Mass Spectrometry Research Laboratory and NIH instrumentation grant S10OD021486.

Author Contributions: Conceptualization, G.V.W.J., T.D., J.E.; Experimentation: T.D., J.E., M.H.; Data Analysis, G.V.W.J., T.D., J.E., M.H.; Manuscript preparation, Review and Editing, G.V.W.J., T.D., J.E., M.H., J.W.K.; Funding Acquisition, G.V.W.J. All authors have read and agreed to the published version of the manuscript.

Conflicts of Interest: The authors declare no conflict of interest.

References

1. Sofroniew, M.V.; Vinters, H.V. Astrocytes: biology and pathology. *Acta Neuropathol* **2010**, *119*, 7-35, doi:10.1007/s00401-009-0619-8.
2. Chung, W.S.; Allen, N.J.; Eroglu, C. Astrocytes Control Synapse Formation, Function, and Elimination. *Cold Spring Harb Perspect Biol* **2015**, *7*, a020370, doi:10.1101/cshperspect.a020370.
3. Barres, B.A. The mystery and magic of glia: a perspective on their roles in health and disease. *Neuron* **2008**, *60*, 430-440, doi:10.1016/j.neuron.2008.10.013.
4. Anderson, M.A.; Ao, Y.; Sofroniew, M.V. Heterogeneity of reactive astrocytes. *Neurosci Lett* **2014**, *565*, 23-29, doi:10.1016/j.neulet.2013.12.030.
5. Burda, J.E.; O'Shea, T.M.; Ao, Y.; Suresh, K.B.; Wang, S.; Bernstein, A.M.; Chandra, A.; Deverasetty, S.; Kawaguchi, R.; Kim, J.H.; et al. Divergent transcriptional regulation of astrocyte reactivity across disorders. *Nature* **2022**, *606*, 557-564, doi:10.1038/s41586-022-04739-5.
6. Escartin, C.; Galea, E.; Lakatos, A.; O'Callaghan, J.P.; Petzold, G.C.; Serrano-Pozo, A.; Steinhauser, C.; Volterra, A.; Carmignoto, G.; Agarwal, A.; et al. Reactive astrocyte nomenclature, definitions, and future directions. *Nat Neurosci* **2021**, *24*, 312-325, doi:10.1038/s41593-020-00783-4.
7. Linnerbauer, M.; Rothhammer, V. Protective Functions of Reactive Astrocytes Following Central Nervous System Insult. *Front Immunol* **2020**, *11*, 573256, doi:10.3389/fimmu.2020.573256.
8. Davies, S.J.; Fitch, M.T.; Memberg, S.P.; Hall, A.K.; Raisman, G.; Silver, J. Regeneration of adult axons in white matter tracts of the central nervous system. *Nature* **1997**, *390*, 680-683, doi:10.1038/37776.
9. Guttenplan, K.A.; Weigel, M.K.; Prakash, P.; Wijewardhane, P.R.; Hasel, P.; Rufen-Blanchette, U.; Munch, A.E.; Blum, J.A.; Fine, J.; Neal, M.C.; et al. Neurotoxic reactive astrocytes induce cell death via saturated lipids. *Nature* **2021**, *599*, 102-107, doi:10.1038/s41586-021-03960-y.
10. Liddelow, S.A.; Guttenplan, K.A.; Clarke, L.E.; Bennett, F.C.; Bohlen, C.J.; Schirmer, L.; Bennett, M.L.; Munch, A.E.; Chung, W.S.; Peterson, T.C.; et al. Neurotoxic reactive astrocytes are induced by activated microglia. *Nature* **2017**, *541*, 481-487, doi:10.1038/nature21029.
11. Smith, G.M.; Strunz, C. Growth factor and cytokine regulation of chondroitin sulfate proteoglycans by astrocytes. *Glia* **2005**, *52*, 209-218, doi:10.1002/glia.20236.
12. Yiu, G.; He, Z. Glial inhibition of CNS axon regeneration. *Nat Rev Neurosci* **2006**, *7*, 617-627, doi:10.1038/nrn1956.
13. Colak, G.; Johnson, G.V. Complete transglutaminase 2 ablation results in reduced stroke volumes and astrocytes that exhibit increased survival in response to ischemia. *Neurobiol Dis* **2012**, *45*, 1042-1050, doi:10.1016/j.nbd.2011.12.023.
14. Elahi, A.; Emerson, J.; Rudlong, J.; Keillor, J.W.; Salois, G.; Visca, A.; Girardi, P.; Johnson, G.V.W.; Proschel, C. Deletion or Inhibition of Astrocytic Transglutaminase 2 Promotes Functional Recovery after Spinal Cord Injury. *Cells* **2021**, *10*, doi:10.3390/cells10112942.
15. Emerson, J.; Delgado, T.; Girardi, P.; Johnson, G.V.W. Deletion of Transglutaminase 2 from Mouse Astrocytes Significantly Improves Their Ability to Promote Neurite Outgrowth on an Inhibitory Matrix. *Int J Mol Sci* **2023**, *24*, doi:ARTN 6058 10.3390/ijms24076058.
16. Feola, J.; Barton, A.; Akbar, A.; Keillor, J.; Johnson, G.V.W. Transglutaminase 2 modulation of NF-kappaB signaling in astrocytes is independent of its ability to mediate astrocytic viability in ischemic injury. *Brain Res* **2017**, *1668*, 1-11, doi:10.1016/j.brainres.2017.05.009.
17. Monteagudo, A.; Feola, J.; Natola, H.; Ji, C.; Proschel, C.; Johnson, G.V.W. Depletion of astrocytic transglutaminase 2 improves injury outcomes. *Mol Cell Neurosci* **2018**, *92*, 128-136, doi:10.1016/j.mcn.2018.06.007.
18. Gundemir, S.; Colak, G.; Tucholski, J.; Johnson, G.V. Transglutaminase 2: a molecular Swiss army knife. *Biochim Biophys Acta* **2012**, *1823*, 406-419, doi:10.1016/j.bbamcr.2011.09.012.
19. Griffin, M.; Casadio, R.; Bergamini, C.M. Transglutaminases: nature's biological glues. *Biochem J* **2002**, *368*, 377-396, doi:10.1042/BJ20021234.

20. Chen, J.S.; Mehta, K. Tissue transglutaminase: an enzyme with a split personality. *Int J Biochem Cell Biol* **1999**, *31*, 817-836, doi:10.1016/s1357-2725(99)00045-x.
21. Farrelly, L.A.; Thompson, R.E.; Zhao, S.; Lepack, A.E.; Lyu, Y.; Bhanu, N.V.; Zhang, B.; Loh, Y.E.; Ramakrishnan, A.; Vadodaria, K.C.; et al. Histone serotonylation is a permissive modification that enhances TFIID binding to H3K4me3. *Nature* **2019**, *567*, 535-539, doi:10.1038/s41586-019-1024-7.
22. Lepack, A.E.; Werner, C.T.; Stewart, A.F.; Fulton, S.L.; Zhong, P.; Farrelly, L.A.; Smith, A.C.W.; Ramakrishnan, A.; Lyu, Y.; Bastle, R.M.; et al. Dopaminylation of histone H3 in ventral tegmental area regulates cocaine seeking. *Science* **2020**, *368*, 197-201, doi:10.1126/science.aaw8806.
23. Keillor, J.W.; Johnson, G.V.W. Transglutaminase 2 as a therapeutic target for neurological conditions. *Expert Opin Ther Targets* **2021**, *25*, 721-731, doi:10.1080/14728222.2021.1989410.
24. Pinkas, D.M.; Strop, P.; Brunger, A.T.; Khosla, C. Transglutaminase 2 undergoes a large conformational change upon activation. *Plos Biol* **2007**, *5*, e327, doi:10.1371/journal.pbio.0050327.
25. Begg, G.E.; Carrington, L.; Stokes, P.H.; Matthews, J.M.; Wouters, M.A.; Husain, A.; Lorand, L.; Iismaa, S.E.; Graham, R.M. Mechanism of allosteric regulation of transglutaminase 2 by GTP. *Proc Natl Acad Sci U S A* **2006**, *103*, 19683-19688, doi:10.1073/pnas.0609283103.
26. Liu, S.; Cerione, R.A.; Clardy, J. Structural basis for the guanine nucleotide-binding activity of tissue transglutaminase and its regulation of transamidation activity. *Proc Natl Acad Sci U S A* **2002**, *99*, 2743-2747, doi:10.1073/pnas.042454899.
27. Akimov, S.S.; Belkin, A.M. Cell-surface transglutaminase promotes fibronectin assembly via interaction with the gelatin-binding domain of fibronectin: a role in TGFbeta-dependent matrix deposition. *J Cell Sci* **2001**, *114*, 2989-3000, doi:10.1242/jcs.114.16.2989.
28. Eckert, R.L.; Kaartinen, M.T.; Nurminskaya, M.; Belkin, A.M.; Colak, G.; Johnson, G.V.; Mehta, K. Transglutaminase regulation of cell function. *Physiol Rev* **2014**, *94*, 383-417, doi:10.1152/physrev.00019.2013.
29. Rossin, F.; Ciccosanti, F.; D'Eletto, M.; Occhigrossi, L.; Fimia, G.M.; Piacentini, M. Type 2 transglutaminase in the nucleus: the new epigenetic face of a cytoplasmic enzyme. *Cell Mol Life Sci* **2023**, *80*, 52, doi:10.1007/s00018-023-04698-8.
30. van Strien, M.E.; Breve, J.J.; Fratantoni, S.; Schreurs, M.W.; Bol, J.G.; Jongenelen, C.A.; Drukarch, B.; van Dam, A.M. Astrocyte-derived tissue transglutaminase interacts with fibronectin: a role in astrocyte adhesion and migration? *PLoS One* **2011**, *6*, e25037, doi:10.1371/journal.pone.0025037.
31. Filiano, A.J.; Tucholski, J.; Dolan, P.J.; Colak, G.; Johnson, G.V. Transglutaminase 2 protects against ischemic stroke. *Neurobiol Dis* **2010**, *39*, 334-343, doi:10.1016/j.nbd.2010.04.018.
32. Ientile, R.; Caccamo, D.; Marciano, M.C.; Curro, M.; Mannucci, C.; Campisi, A.; Calapai, G. Transglutaminase activity and transglutaminase mRNA transcripts in gerbil brain ischemia. *Neurosci Lett* **2004**, *363*, 173-177, doi:10.1016/j.neulet.2004.04.003.
33. Ientile, R.; Curro, M.; Caccamo, D. Transglutaminase 2 and neuroinflammation. *Amino Acids* **2015**, *47*, 19-26, doi:10.1007/s00726-014-1864-2.
34. Quinn, B.R.; Yunes-Medina, L.; Johnson, G.V.W. Transglutaminase 2: Friend or foe? The discordant role in neurons and astrocytes. *J Neurosci Res* **2018**, *96*, 1150-1158, doi:10.1002/jnr.24239.
35. Galtrey, C.M.; Fawcett, J.W. The role of chondroitin sulfate proteoglycans in regeneration and plasticity in the central nervous system. *Brain Res Rev* **2007**, *54*, 1-18, doi:10.1016/j.brainresrev.2006.09.006.
36. Kurihara, D.; Yamashita, T. Chondroitin sulfate proteoglycans down-regulate spine formation in cortical neurons by targeting tropomyosin-related kinase B (TrkB) protein. *J Biol Chem* **2012**, *287*, 13822-13828, doi:10.1074/jbc.M111.314070.
37. Akbar, A.; McNeil, N.M.R.; Albert, M.R.; Ta, V.; Adhikary, G.; Bourgeois, K.; Eckert, R.L.; Keillor, J.W. Structure-Activity Relationships of Potent, Targeted Covalent Inhibitors That Abolish Both the Transamidation and GTP Binding Activities of Human Tissue Transglutaminase. *J Med Chem* **2017**, *60*, 7910-7927, doi:10.1021/acs.jmedchem.7b01070.
38. Gundemir, S.; Monteagudo, A.; Akbar, A.; Keillor, J.W.; Johnson, G.V.W. The complex role of transglutaminase 2 in glioblastoma proliferation. *Neuro-Oncology* **2017**, *19*, 208-218, doi:10.1093/neuonc/now157.

39. Mironov, G.G.; Clouthier, C.M.; Akbar, A.; Keillor, J.W.; Berezovski, M.V. Simultaneous analysis of enzyme structure and activity by kinetic capillary electrophoresis-MS. *Nat Chem Biol* **2016**, *12*, 918-922, doi:10.1038/nchembio.2170.
40. Kerr, C.; Szmacinski, H.; Fisher, M.L.; Nance, B.; Lakowicz, J.R.; Akbar, A.; Keillor, J.W.; Lok Wong, T.; Godoy-Ruiz, R.; Toth, E.A.; et al. Transamidase site-targeted agents alter the conformation of the transglutaminase cancer stem cell survival protein to reduce GTP binding activity and cancer stem cell survival. *Oncogene* **2017**, *36*, 2981-2990, doi:10.1038/onc.2016.452.
41. Ji, C.; Tang, M.; Harrison, J.; Paciorkowski, A.; Johnson, G.V.W. Nuclear transglutaminase 2 directly regulates expression of cathepsin S in rat cortical neurons. *Eur J Neurosci* **2018**, *48*, 3043-3051, doi:10.1111/ejn.14159.
42. Gundemir, S.; Colak, G.; Feola, J.; Blouin, R.; Johnson, G.V. Transglutaminase 2 facilitates or ameliorates HIF signaling and ischemic cell death depending on its conformation and localization. *Biochim Biophys Acta* **2013**, *1833*, 1-10, doi:10.1016/j.bbamcr.2012.10.011.
43. McAlister, G.C.; Nusinow, D.P.; Jedrychowski, M.P.; Wuhr, M.; Huttlin, E.L.; Erickson, B.K.; Rad, R.; Haas, W.; Gygi, S.P. MultiNotch MS3 enables accurate, sensitive, and multiplexed detection of differential expression across cancer cell line proteomes. *Anal Chem* **2014**, *86*, 7150-7158, doi:10.1021/ac502040v.
44. Demichev, V.; Messner, C.B.; Vernardis, S.I.; Lilley, K.S.; Ralser, M. DIA-NN: neural networks and interference correction enable deep proteome coverage in high throughput. *Nat Methods* **2020**, *17*, 41-44, doi:10.1038/s41592-019-0638-x.
45. Cox, J.; Hein, M.Y.; Luber, C.A.; Paron, I.; Nagaraj, N.; Mann, M. Accurate proteome-wide label-free quantification by delayed normalization and maximal peptide ratio extraction, termed MaxLFQ. *Mol Cell Proteomics* **2014**, *13*, 2513-2526, doi:10.1074/mcp.M113.031591.
46. Tyanova, S.; Temu, T.; Sinitcyn, P.; Carlson, A.; Hein, M.Y.; Geiger, T.; Mann, M.; Cox, J. The Perseus computational platform for comprehensive analysis of (prote)omics data. *Nat Methods* **2016**, *13*, 731-740, doi:10.1038/nmeth.3901.
47. Basso, M.; Ratan, R.R. Transglutaminase is a therapeutic target for oxidative stress, excitotoxicity and stroke: a new epigenetic kid on the CNS block. *J Cereb Blood Flow Metab* **2013**, *33*, 809-818, doi:10.1038/jcbfm.2013.53.
48. Colak, G.; Keillor, J.W.; Johnson, G.V. Cytosolic guanine nucledotide binding deficient form of transglutaminase 2 (R580a) potentiates cell death in oxygen glucose deprivation. *PLoS One* **2011**, *6*, e16665, doi:10.1371/journal.pone.0016665.
49. Filiano, A.J.; Bailey, C.D.; Tucholski, J.; Gundemir, S.; Johnson, G.V. Transglutaminase 2 protects against ischemic insult, interacts with HIF1beta, and attenuates HIF1 signaling. *FASEB J* **2008**, *22*, 2662-2675, doi:10.1096/fj.07-097709.
50. Gundemir, S.; Johnson, G.V. Intracellular localization and conformational state of transglutaminase 2: implications for cell death. *PLoS One* **2009**, *4*, e6123, doi:10.1371/journal.pone.0006123.
51. McConoughey, S.J.; Basso, M.; Niatsetskaya, Z.V.; Sleiman, S.F.; Smirnova, N.A.; Langley, B.C.; Mahishi, L.; Cooper, A.J.; Antonyak, M.A.; Cerione, R.A.; et al. Inhibition of transglutaminase 2 mitigates transcriptional dysregulation in models of Huntington disease. *EMBO Mol Med* **2010**, *2*, 349-370, doi:10.1002/emmm.201000084.
52. Milakovic, T.; Tucholski, J.; McCoy, E.; Johnson, G.V. Intracellular localization and activity state of tissue transglutaminase differentially impacts cell death. *J Biol Chem* **2004**, *279*, 8715-8722, doi:10.1074/jbc.M308479200.
53. Rroji, O.; Kumar, A.; Karuppagounder, S.S.; Ratan, R.R. Epigenetic regulators of neuronal ferroptosis identify novel therapeutics for neurological diseases: HDACs, transglutaminases, and HIF prolyl hydroxylases. *Neurobiol Dis* **2021**, *147*, 105145, doi:10.1016/j.nbd.2020.105145.
54. Tatsukawa, H.; Furutani, Y.; Hitomi, K.; Kojima, S. Transglutaminase 2 has opposing roles in the regulation of cellular functions as well as cell growth and death. *Cell Death Dis* **2016**, *7*, e2244, doi:10.1038/cddis.2016.150.

55. Kim, H.J.; Lee, J.H.; Cho, S.Y.; Jeon, J.H.; Kim, I.G. Transglutaminase 2 mediates transcriptional regulation through BAF250a polyamination. *Genes Genomics* **2021**, *43*, 333-342, doi:10.1007/s13258-021-01055-6.
56. Pittol, J.M.R.; Oruba, A.; Mittler, G.; Saccani, S.; van Essen, D. Zbtb7a is a transducer for the control of promoter accessibility by NF-kappa B and multiple other transcription factors. *Plos Biol* **2018**, *16*, doi:ARTN e2004526 10.1371/journal.pbio.2004526.
57. Choi, W.I.; Jeon, B.N.; Yun, C.O.; Kim, P.H.; Kim, S.E.; Choi, K.Y.; Kim, S.H.; Hur, M.W. Proto-oncogene FBI-1 represses transcription of p21CIP1 by inhibition of transcription activation by p53 and Sp1. *J Biol Chem* **2009**, *284*, 12633-12644, doi:10.1074/jbc.M809794200.
58. Kadamb, R.; Mittal, S.; Bansal, N.; Batra, H.; Saluja, D. Sin3: insight into its transcription regulatory functions. *Eur J Cell Biol* **2013**, *92*, 237-246, doi:10.1016/j.ejcb.2013.09.001.
59. Laudes, M.; Bilkovski, R.; Oberhauser, F.; Droste, A.; Gomolka, M.; Leeser, U.; Udelhoven, M.; Krone, W. Transcription factor FBI-1 acts as a dual regulator in adipogenesis by coordinated regulation of cyclin-A and E2F-4. *J Mol Med (Berl)* **2008**, *86*, 597-608, doi:10.1007/s00109-008-0326-2.
60. Yunes-Medina, L.; Feola, J.; Johnson, G.V.W. Subcellular localization patterns of transglutaminase 2 in astrocytes and neurons are differentially altered by hypoxia. *Neuroreport* **2017**, *28*, 1208-1214, doi:10.1097/WNR.0000000000000895.
61. Tiana, M.; Acosta-Iborra, B.; Puente-Santamaria, L.; Hernansanz-Agustin, P.; Worsley-Hunt, R.; Masson, N.; Garcia-Rio, F.; Mole, D.; Ratcliffe, P.; Wasserman, W.W.; et al. The SIN3A histone deacetylase complex is required for a complete transcriptional response to hypoxia. *Nucleic Acids Res* **2018**, *46*, 120-133, doi:10.1093/nar/gkx951.
62. Icardi, L.; Mori, R.; Gesellchen, V.; Eyckerman, S.; De Cauwer, L.; Verhelst, J.; Vercauteren, K.; Saelens, X.; Meuleman, P.; Leroux-Roels, G.; et al. The Sin3a repressor complex is a master regulator of STAT transcriptional activity. *Proc Natl Acad Sci U S A* **2012**, *109*, 12058-12063, doi:10.1073/pnas.1206458109.
63. Gates, L.A.; Shi, J.; Rohira, A.D.; Feng, Q.; Zhu, B.; Bedford, M.T.; Sagum, C.A.; Jung, S.Y.; Qin, J.; Tsai, M.J.; et al. Acetylation on histone H3 lysine 9 mediates a switch from transcription initiation to elongation. *J Biol Chem* **2017**, *292*, 14456-14472, doi:10.1074/jbc.M117.802074.
64. Sakamoto, K.; Ozaki, T.; Ko, Y.C.; Tsai, C.F.; Gong, Y.; Morozumi, M.; Ishikawa, Y.; Uchimura, K.; Nadanaka, S.; Kitagawa, H.; et al. Glycan sulfation patterns define autophagy flux at axon tip via PTPRsigma-cortactin axis. *Nat Chem Biol* **2019**, *15*, 699-709, doi:10.1038/s41589-019-0274-x.
65. He, F.; Ru, X.; Wen, T. NRF2, a Transcription Factor for Stress Response and Beyond. *Int J Mol Sci* **2020**, *21*, doi:10.3390/ijms21134777.
66. Habas, A.; Hahn, J.; Wang, X.; Margeta, M. Neuronal activity regulates astrocytic Nrf2 signaling. *Proc Natl Acad Sci U S A* **2013**, *110*, 18291-18296, doi:10.1073/pnas.1208764110.
67. Vargas, M.R.; Johnson, J.A. The Nrf2-ARE cytoprotective pathway in astrocytes. *Expert Rev Mol Med* **2009**, *11*, e17, doi:10.1017/S1462399409001094.
68. Zhao, W.; Gasterich, N.; Clarner, T.; Voelz, C.; Behrens, V.; Beyer, C.; Fragoulis, A.; Zendedel, A. Astrocytic Nrf2 expression protects spinal cord from oxidative stress following spinal cord injury in a male mouse model. *J Neuroinflammation* **2022**, *19*, 134, doi:10.1186/s12974-022-02491-1.
69. Margueron, R.; Reinberg, D. The Polycomb complex PRC2 and its mark in life. *Nature* **2011**, *469*, 343-349, doi:10.1038/nature09784.

Figure Legends

Figure 1. VA4 inhibition of TG2 facilitates the ability of WT astrocytes to promote neurite outgrowth on a chondroitin sulfate proteoglycan (CSPG) growth-inhibitory matrix. (a) Schematic of neurite outgrowth experimental paradigm including VA4 treatment. Created with BioRender.com. (b) Representative images of MAP2 staining of neurons without paired astrocytes, neurons paired with vehicle (DMSO)-treated astrocytes, or neurons paired with VA4-treated astrocytes (scale bar = 20 µm). (c) Quantification of length of longest neurite for neuron experimental groups on CSPG matrix. Shown as Mean and SEM (n= 86-111 neurons per group from two biological replicates, Kruskal Wallis Test **$p < 0.01$, ****$p < 0.0001$).

Figure 2. Irreversible inhibition of TG2 with the drug VA4 reduces interaction between TG2 and Zbtb7a. (a) Input controls of V5-TG2 and FLAG-Zbtb7a transfected into HEK 293TN cells treated with VA4 or vehicle control (DMSO). (b) Immunoprecipitation of V5-TG2 pulls down less FLAG-Zbtb7a in cell lysates that were treated with VA4. In (a) and (b) the position at which molecular weight markers (kDa) migrated is indicated at the left of the immunoblots. (c) Quantification of the amount of FLAG-Zbtb7a pulled down normalized to the amount of V5-TG2 immunoprecipitated. Treatment of cells with VA4 resulted in a significant reduction in the Zbtb7a co-immunoprecipitated with TG2 compared to DMSO control. Shown as mean and SEM (n=5 samples per condition from 4 independent biological replicates, unpaired t-test ***$p < 0.001$).

Figure 3. TG2-/- astrocytes have significantly greater acetylation of histone H3 at lysine residue 9 (H3K9ac) compared to WT astrocytes. (a) Representative western blot of WT and TG2-/- astrocyte lysates probed for Histone H3 acetylated at lysine residue 9 (H3K9ac). The position at which molecular weight markers (kDa) migrated is indicated at the left of the immunoblots. (b) Quantification of H3K9ac levels in WT and TG2-/- astrocytes. TG2-/- astrocytes showed significantly greater acetylation of H3K9 than WT astrocytes (~60%). Shown as mean and SEM (n=1-4 samples per condition from 4 independent biological replicates, unpaired t-test **$p< 0.01$).

Figure 4. WT astrocytes treated with VA4 show significantly greater H3K9 acetylation compared to DMSO vehicle control treated WT astrocytes. (a) Western blot of 10 µM VA4- and DMSO-treated WT astrocyte lysates probed for H3K9ac. The position at which molecular weight markers (kDa) migrated is indicated at the left of the

immunoblots. (b) Quantification of H3K9ac levels showed significantly greater acetylation in VA4-treated WT astrocytes compared to DMSO-treated WT astrocytes (~65%). Shown as Mean and SEM (n=3 samples per condition from 2 independent biological replicates, unpaired t-test *p< 0.01).

Figure 5. TG2-/- and VA4-treated astrocytes share significant alterations in proteins associated with lipid metabolic and antioxidant pathways. (a) Volcano plot of significant differentially regulated proteins comparing TG2-/- to WT astrocyte cultures (n=5 samples per condition from 1 biological replicate) with thresholds set for log2 fold changes at +/- 0.5 and for adjusted p value < 0.05, and (b) DAVID GO Biological Process analysis of up- and down-regulated proteins. (c) Volcano plot of significant differentially regulated proteins comparing VA4-treated to DMSO-treated WT astrocyte cultures (n=6 samples per condition from 2 independent biological replicates) with thresholds set as above, and (d) DAVID GO Biological Process analysis of up- and down-regulated proteins. (e-f) Enrichr transcription factor enrichment of up- and down-regulated proteins in (e) TG2-/- astrocytes (f) VA4-treated astrocytes. (g) Venn diagram showing overlap of significant differentially regulated proteins in both TG2-/- and VA4 datasets.

Figure 6. Proposed mechanism by which TG2 modulates the neuroprotective phenotype of reactive astrocytes. In stressed astrocytes, TG2 is able to move in and out of the nucleus. While in the nucleus, TG2 can interact with Zbtb7a and Sin3a, resulting in increased histone deacetylase (HDAC) activity and neurosupportive gene repression. If TG2 is deleted from the astrocytes, or the astrocytes are treated with VA4, the recruitment of Zbtb7a/Sin3a/HDAC to the DNA is diminished, resulting in de-repression of neurosupportive genes leading to a more neurosupportive phenotype. The “?” indicates that the effect of VA4 treatment on the nuclear/cytosolic localization of TG2 is unclear. Created with BioRender.com.

Figure 1

(a)

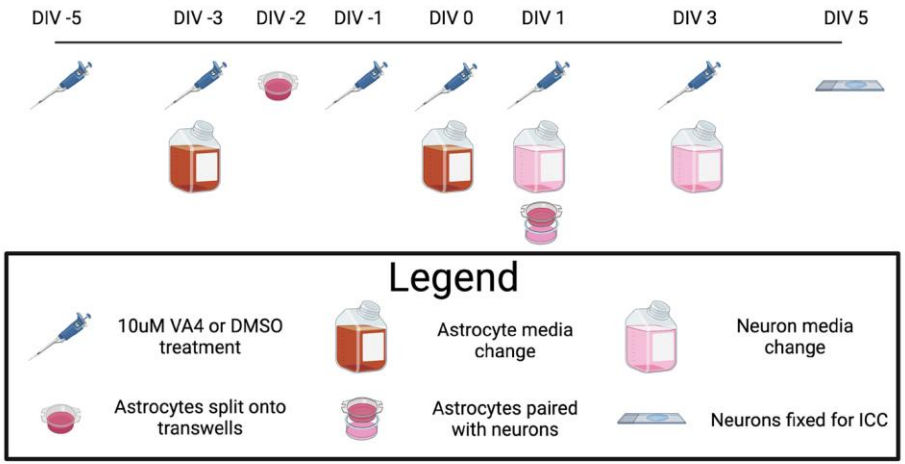
DIV -5
DIV -3
DIV -2
DIV -1
DIV 0
DIV 1
DIV 3
DIV 5
Legend
10uM VA4 or DMSO treatment
Astrocyte media change
Neuron media change
Astrocytes split onto transwells
Astrocytes paired with neurons
Neurons fixed for ICC

(b)

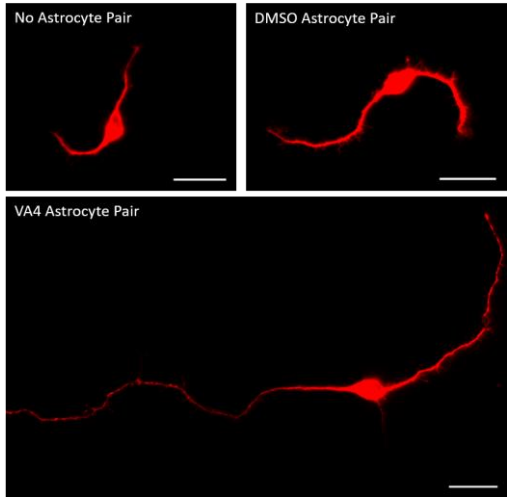
No Astrocyte Pair
DMSO Astrocyte Pair
VA4 Astrocyte Pair

(c)

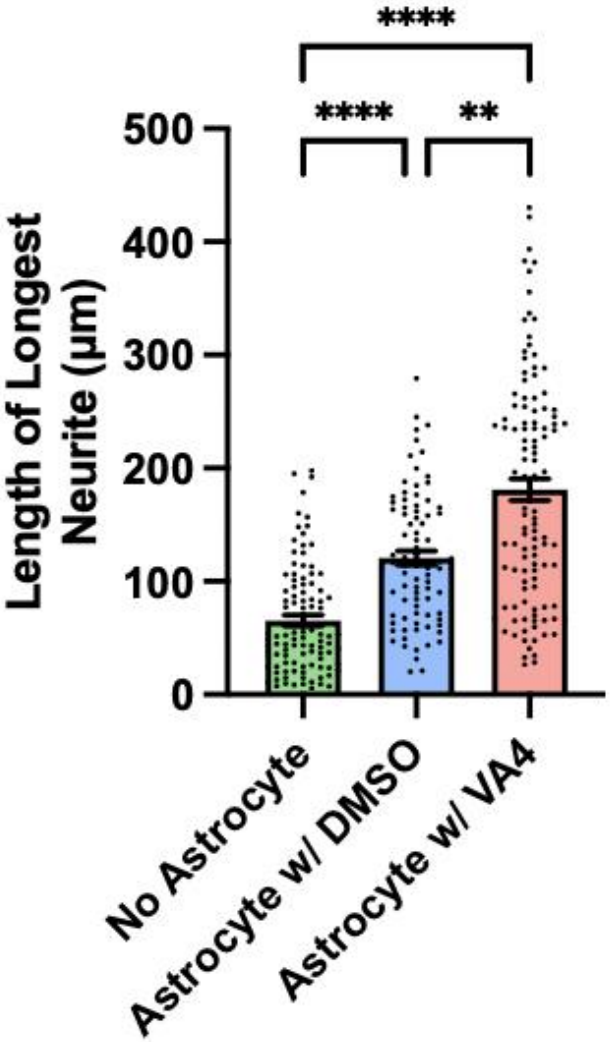
****
****
**
Length of Longest Neurite (µm)
500
400
300
200
100
0
No Astrocyte
Astrocyte w/ DMSO
Astrocyte w/ VA4

Figure 2

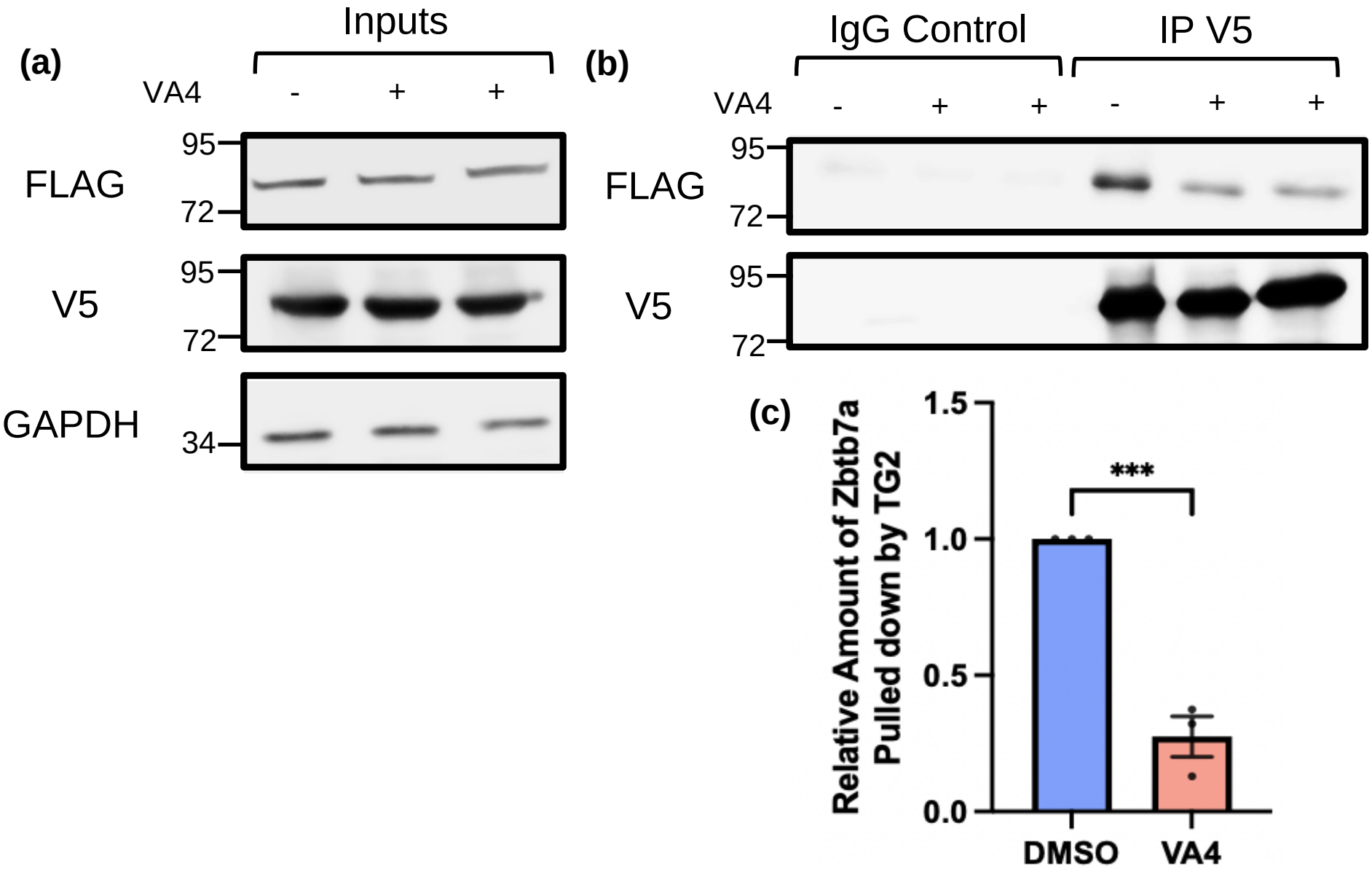
(a)
Inputs
VA4
-
+
+
FLAG
95
72
V5
95
72
GAPDH
34
(b)
IgG Control
IP V5
VA4
-
+
+
-
+
+
FLAG
95
72
V5
95
72
(c)
Relative Amount of Zbtb7a Pulled down by TG2
1.5
1.0
0.5
0.0
***
DMSO
VA4

Figure 3

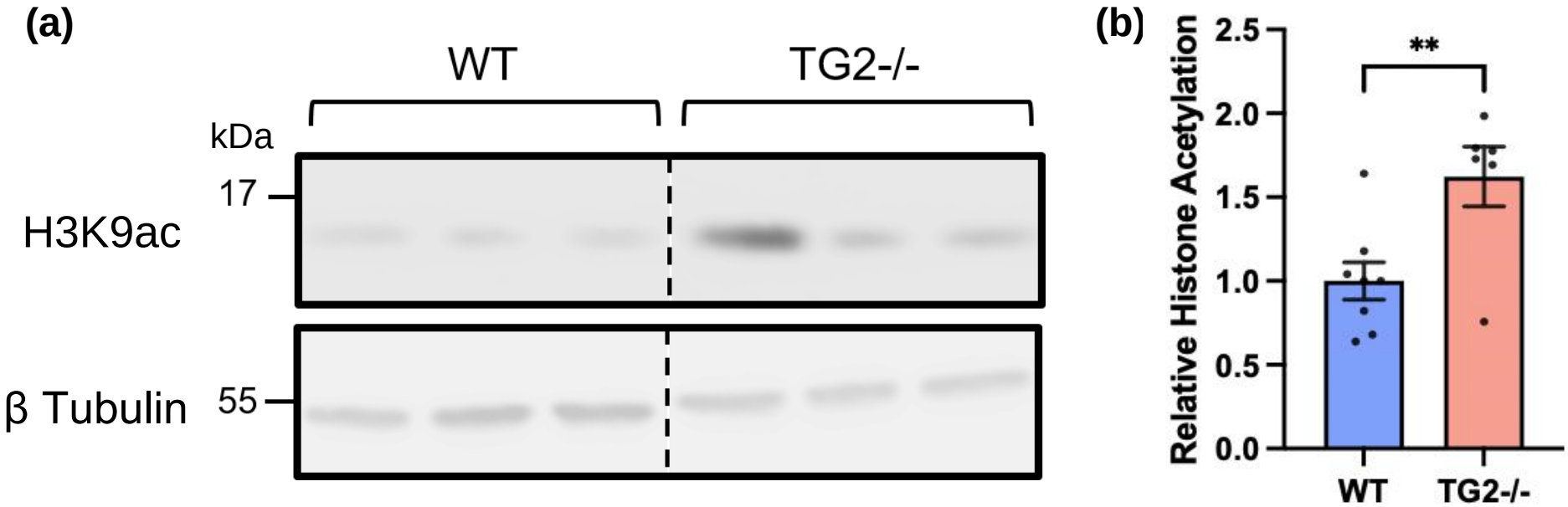
(a)
WT
TG2-/-
kDa
17
H3K9ac
55
β Tubulin
(b)
Relative Histone Acetylation
2.5
2.0
1.5
1.0
0.5
0.0
**
WT
TG2-/-

Figure 4

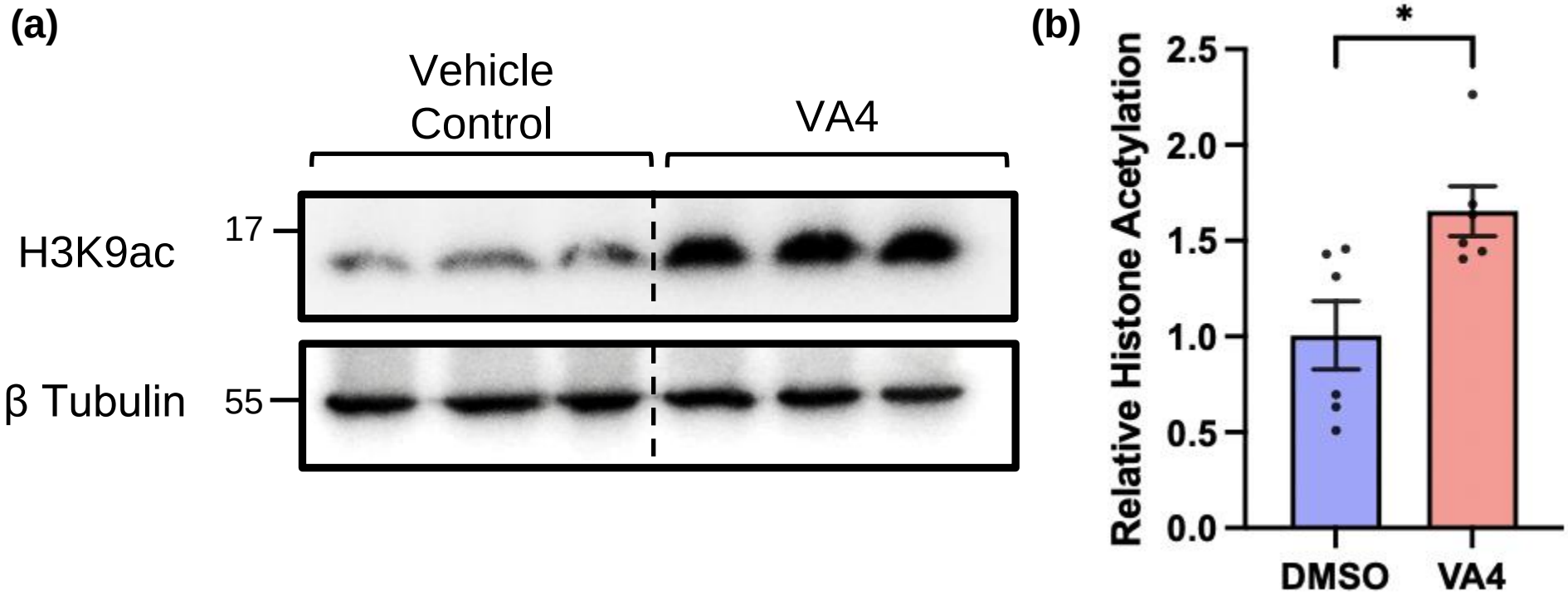
(a)
Vehicle Control
VA4
H3K9ac
17
β Tubulin
55
(b)
*
Relative Histone Acetylation
2.5
2.0
1.5
1.0
0.5
0.0
DMSO
VA4

Figure 5

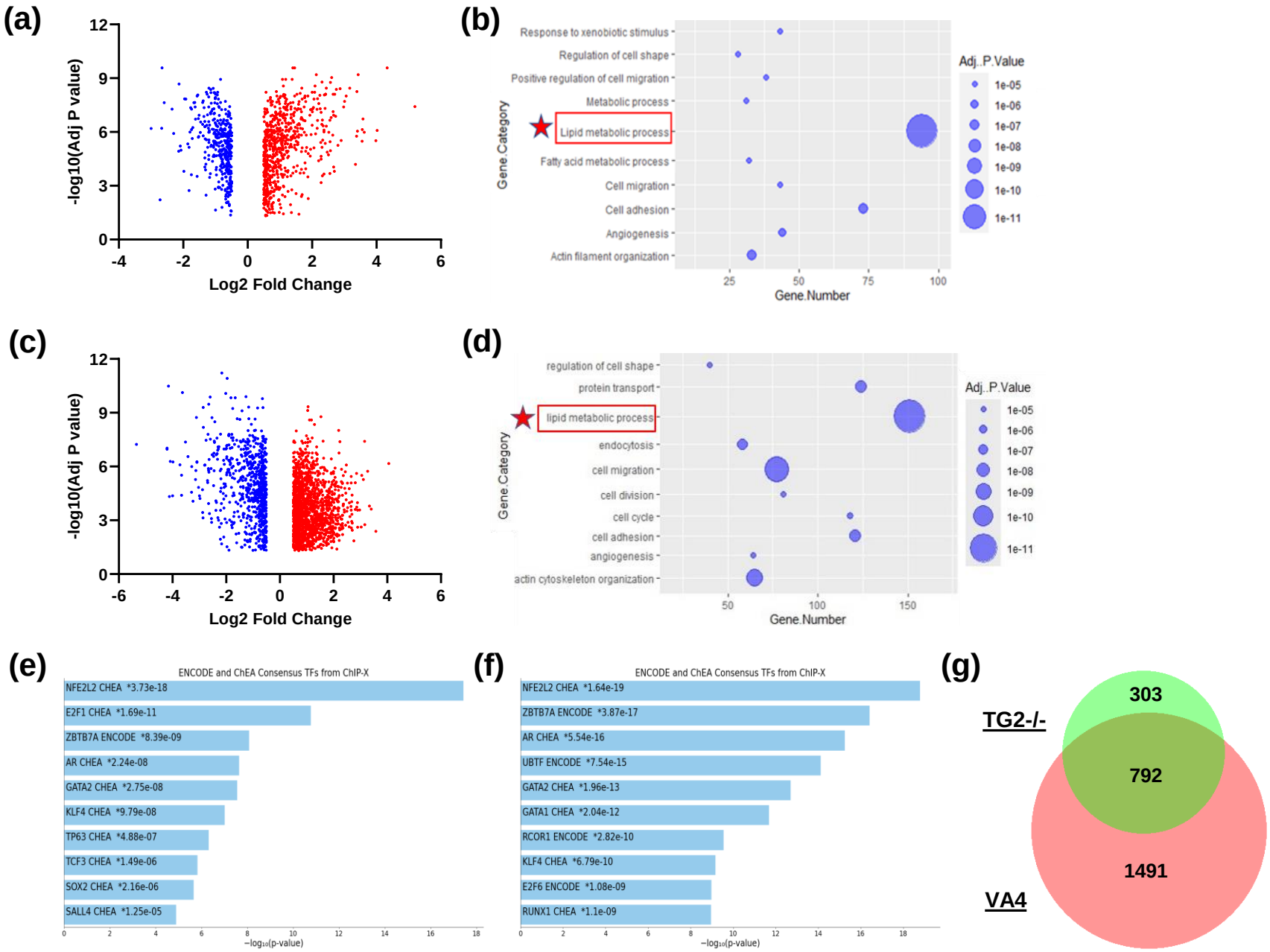
(a)
-log10(Adj P value)
Log2 Fold Change
(b)
Response to xenobiotic stimulus
Regulation of cell shape
Positive regulation of cell migration
Metabolic process
Lipid metabolic process
Fatty acid metabolic process
Cell migration
Cell adhesion
Angiogenesis
Actin filament organization
Gene.Category
Gene.Number
Adj..P.Value
1e-05
1e-06
1e-07
1e-08
1e-09
1e-10
1e-11
(c)
-log10(Adj P value)
Log2 Fold Change
(d)
regulation of cell shape
protein transport
lipid metabolic process
endocytosis
cell migration
cell division
cell cycle
cell adhesion
angiogenesis
actin cytoskeleton organization
Gene.Category
Gene.Number
Adj..P.Value
1e-05
1e-06
1e-07
1e-08
1e-09
1e-10
1e-11
(e)
ENCODE and ChEA Consensus TFs from ChIP-X
NFE2L2 CHEA *3.73e-18
E2F1 CHEA *1.69e-11
ZBTB7A ENCODE *8.39e-09
AR CHEA *2.24e-08
GATA2 CHEA *2.75e-08
KLF4 CHEA *9.79e-08
TP63 CHEA *4.88e-07
TCF3 CHEA *1.49e-06
SOX2 CHEA *2.16e-06
SALL4 CHEA *1.25e-05
−log₁₀(p-value)
(f)
ENCODE and ChEA Consensus TFs from ChIP-X
NFE2L2 CHEA *1.64e-19
ZBTB7A ENCODE *3.87e-17
AR CHEA *5.54e-16
UBTF ENCODE *7.54e-15
GATA2 CHEA *1.96e-13
GATA1 CHEA *2.04e-12
RCOR1 ENCODE *2.82e-10
KLF4 CHEA *6.79e-10
E2F6 ENCODE *1.08e-09
RUNX1 CHEA *1.1e-09
−log₁₀(p-value)
(g)
TG2-/-
VA4
303
792
1491

Figure 6

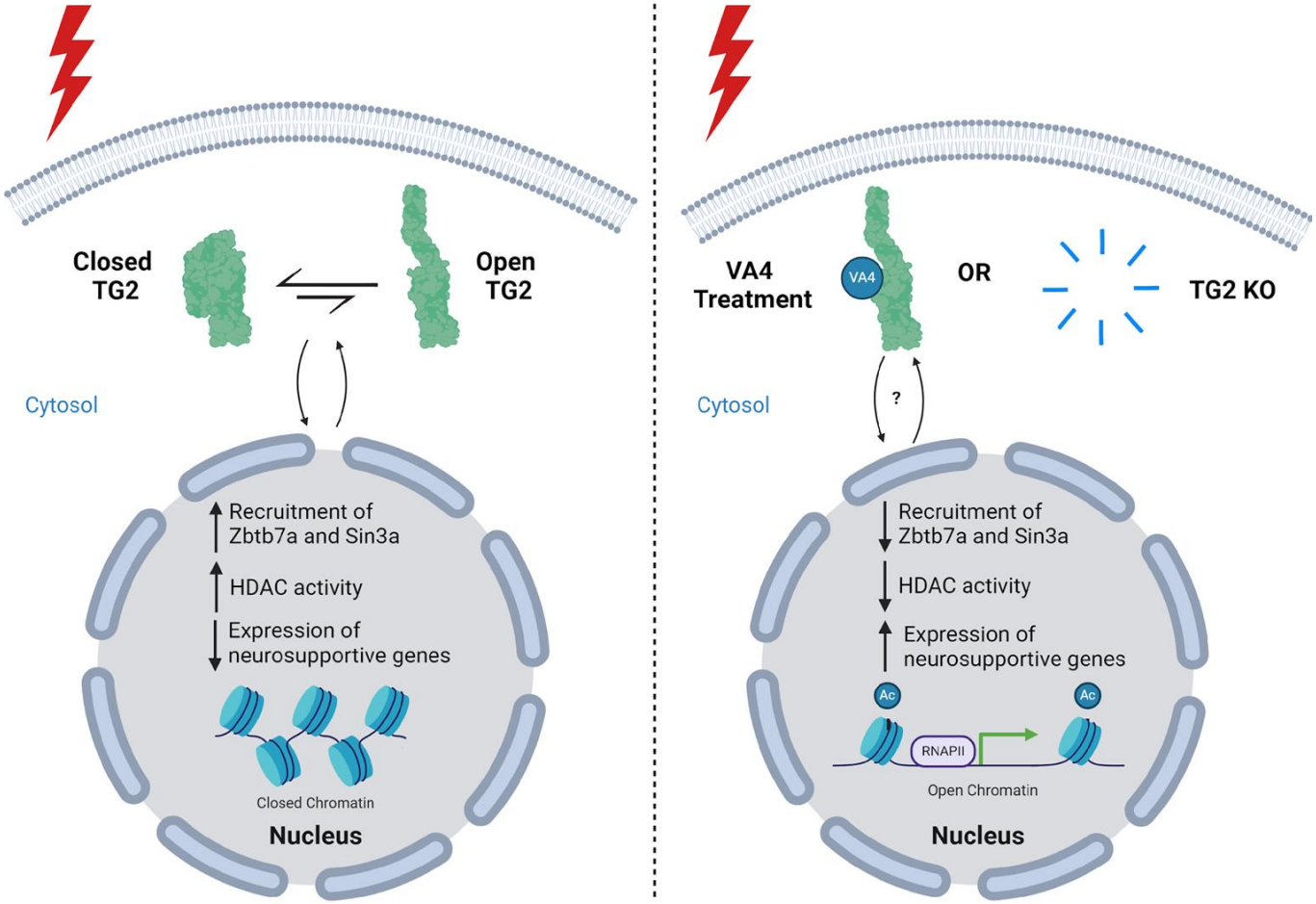
Closed
TG2
Open
TG2
Cytosol
Recruitment of
Zbtb7a and Sin3a
HDAC activity
Expression of
neurosupportive genes
Closed Chromatin
Nucleus
VA4
Treatment
VA4
OR
TG2 KO
Cytosol
?
Recruitment of
Zbtb7a and Sin3a
HDAC activity
Expression of
neurosupportive genes
Ac
Ac
RNAPII
Open Chromatin
Nucleus

Supplemental Figures

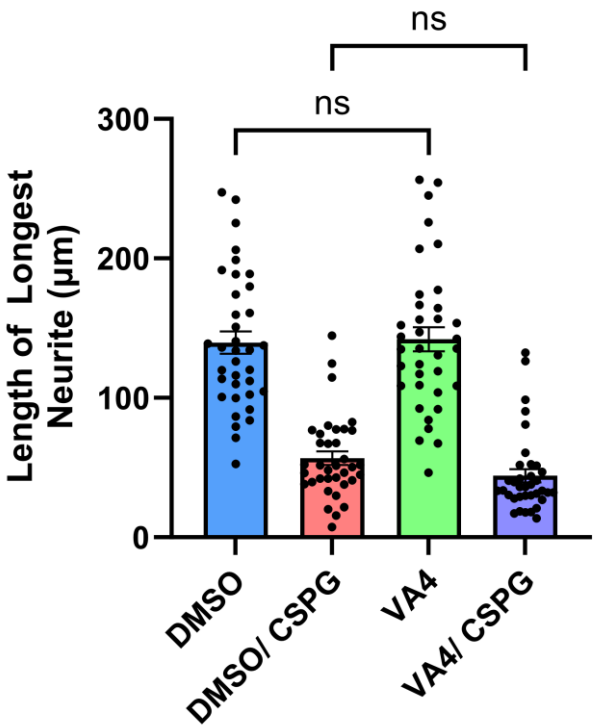

Figure S1. VA4 treatment of neurons does not affect neurite outgrowth on poly D lysine (PDL) or chondroitin sulfate proteoglycan (CSPG) matrices. Neurons were directly treated with DMSO (control) or 10 µM VA4 for 4 days prior to quantification of neurite length on PDL or CSPG matrices. Shown as Mean and SEM (n=36 neurons per condition from 1 biological replicate, Two-way ANOVA).

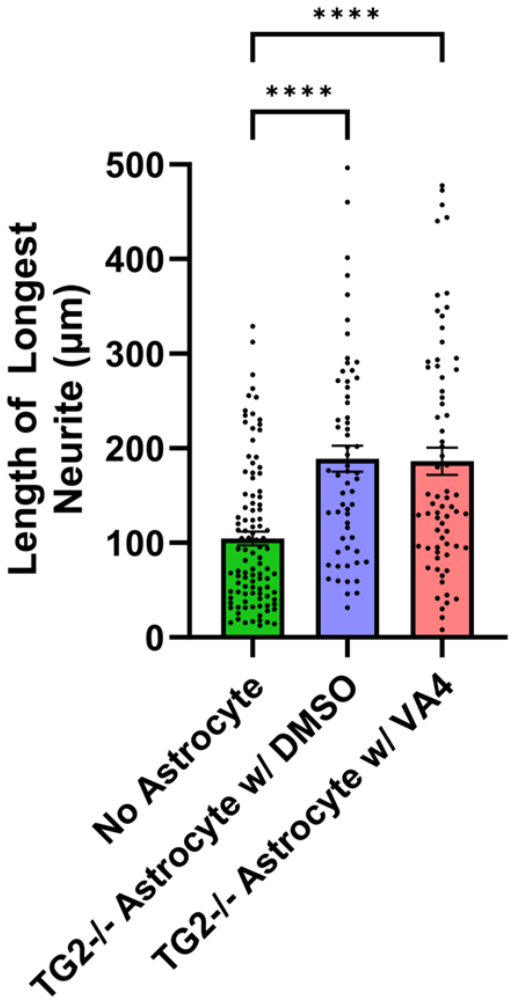

Figure S2. VA4 treatment of TG2-/- astrocytes does not further facilitate their ability to promote neurite outgrowth on chondroitin sulfate proteoglycan (CSPG) matrices. Astrocytes were treated with DMSO (control) or 10 µM VA4 for 4 days prior to pairing with neurons on CSPG matrices. Shown as Mean and SEM (n=61-106 neurons per condition from 1 biological replicate, Kruskal-Wallis Test).

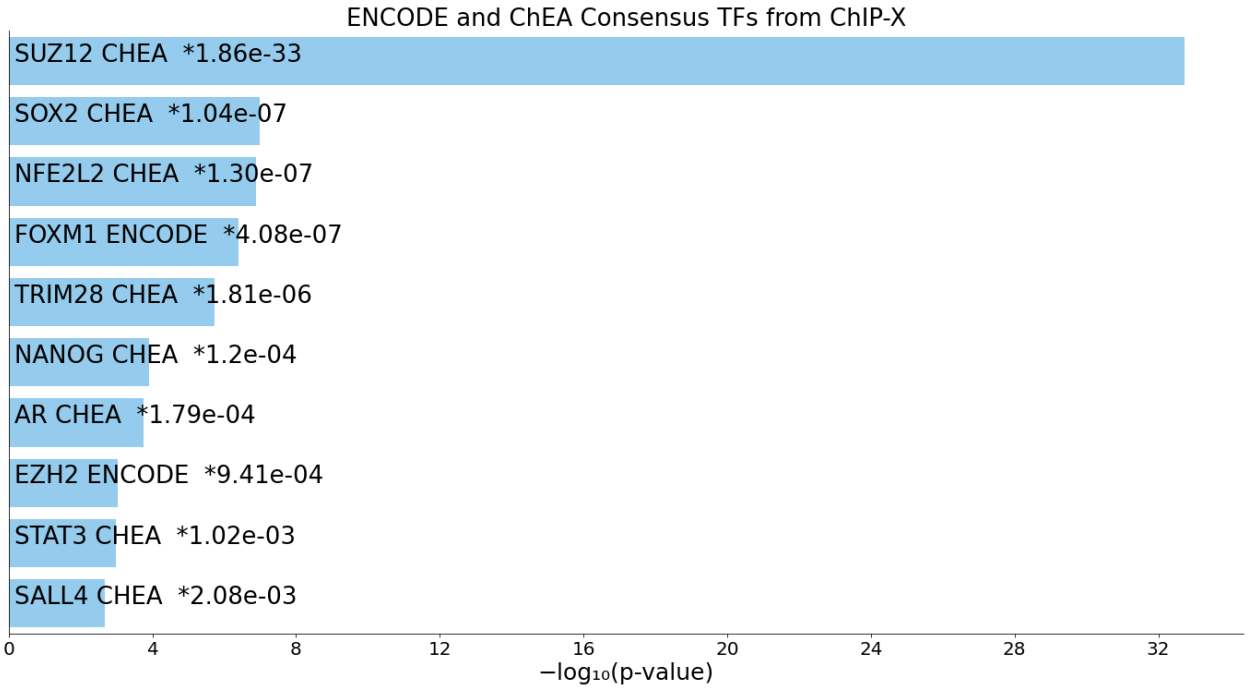

Figure S3. Enrichr transcription factor gene ontology of differentially expressed genes in TG2-/- astrocytes from previous RNA-seq data (Monteagudo et al., 2018) shows a strong enrichment in genes associated with PRC2 repressive chromatin modifying complex components (SUZ12 and EZH2) .

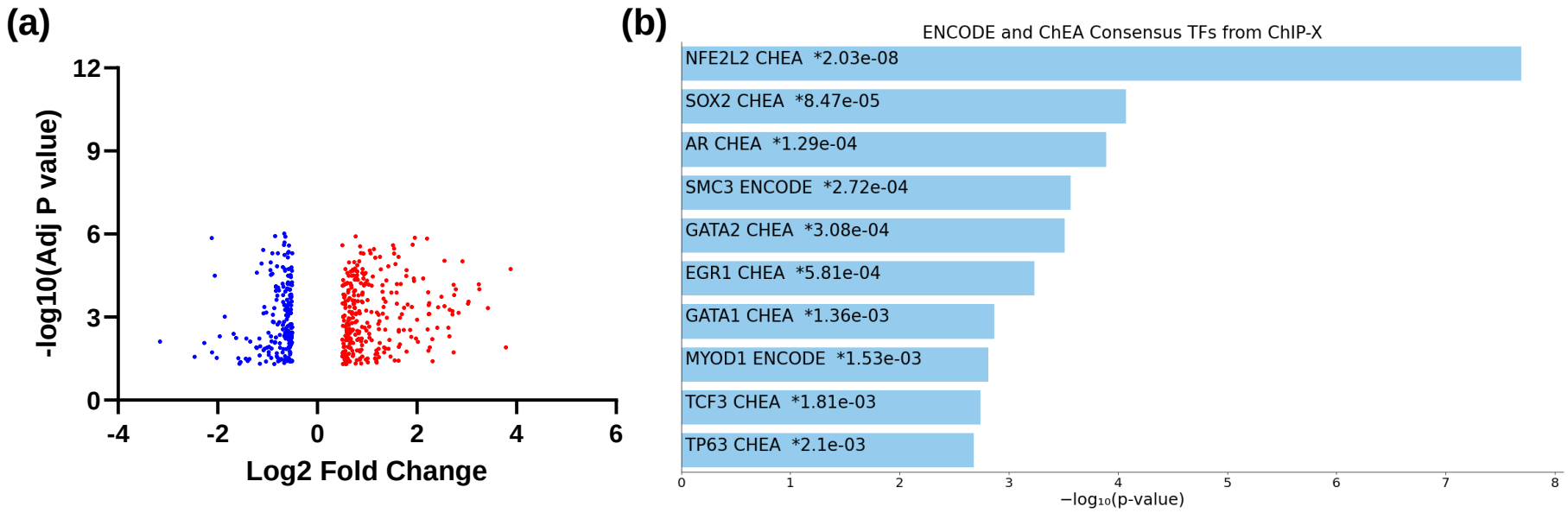

Figure S4. Replicate proteomic analysis of TG2-/- and WT astrocytes using data independent acquisition (DIA). Fold change represents the protein abundance ratio in TG2-/- astrocytes to WT astrocytes. Adj P value was calculated using Benjamini-Hochberg correction for multiple comparisons. Each experimental group contains two biological replicates with 3 technical replicates each for a total of 6 replicates per group.

Table S5. Detailed report of statistical methods used for each figure.

	Normality Test p-value	# Outliers Removed	Test	Sided	Multiple Comparison Correction?	DF	Test Statistic	p-value
Figure 1c	p=0.1719, p=0.0911, p=0.0008	3, 0, 0	Kruskal Wallis Test	N/A	Dunn's multiple comparisons test	3, 300	Z=5.814, Z=9.621, Z=3.251	p<0.0001, p<0.0001, p=0.0034
Figure 2c	p=0.3859	0, 0	Unpaired T test	two	N/A	7	t=13.61	p<0.0001
Figure 3b	p=0.3387, p=0.2143	0, 1	Unpaired T test	two	N/A	11	t=5.312	p=0.0002
Figure 4b	p=0.0917, p=0.0514	0, 0	Unpaired T test	two	N/A	3	t=7.528	p=0.0049
Figure S1	p=0.2708, p=0.0103, p=0.1961, p=0.0017	0, 0, 0, 3	Two-way ANOVA	one	Šídák's multiple comparisons test	35, 3, 102	F (35, 102) =1.191 F (3, 102) = 66.88	p=0.2473 p<0.0001
Figure S2	p=0.0001 p=0.0123 p=0.0004	2, 0, 0	Kruskal Wallis Test	N/A	Dunn's multiple comparisons test	3, 234	Z=5.277 Z=4.909 Z=0.5256	p<0.0001 p<0.0001 p>0.9999